Viral delivery of C9ORF72 hexanucleotide repeat expansions in mice lead to repeat length dependent neuropathology and behavioral deficits

Viral delivery of C9ORF72 hexanucleotide repeat expansions in mice lead to repeat length dependent neuropathology and behavioral deficits.

Saul Herranz-Martin[1#], Jayanth S. Chandran[1#], Katherine Lewis[1], Padraig Mulcahy[1], Adrian Higginbottom[1], Callum Walker[1,2], Isabel Martinez-Pena y Valenzuela[3], Ross A. Jones[4], Ian Coldicott[1], Tommaso Iannitti[1], Mohammed Akaaboune[3], Sherif F. El-Khamisy[2], Thomas H. Gillingwater[4], Pamela J. Shaw[1§] and Mimoun Azzouz[1§*].

[1]Department of Neuroscience, Sheffield Institute for Translational Neuroscience (SITraN), The University of Sheffield, 385A Glossop Road, Sheffield S10 2HQ, UK

[2]Department of Molecular Biology and Biotechnology, Krebs and Sheffield Institute for Nucleic Acids, Firth Court, University of Sheffield, S10 2TN, Sheffield, UK

[3]Molecular, Cellular and Developmental Biology, University of Michigan, 830 North University, Ann Arbor, MI 48109-1048, USA

[4]Centre for Integrative Physiology & Euan MacDonald Centre for Motor Neurone Disease Research,, Hugh Robson Building, The University of Edinburgh, 15 George Square, Edinburgh EH8 9XD, UK

# Authors contributed equally

§ Senior authors

* Correspondence should be addressed to Mimoun Azzouz Email: m.azzouz@sheffield.ac.uk

Keywords: C9orf72, neurodegeneration, ALS/FTD, mouse model, c9RAN aggregates

Running title: C9ORF72 repeat length dependent defects in mice

Summary statement

We have uncoupled the relationship between C9orf72 linked motor neuron disease pathologies by expressing GGGGCC repeat expansions in mice.

Abstract

Intronic GGGGCC repeat expansions in *C9orf72* are the most common genetic cause of amyotrophic lateral sclerosis (ALS) and frontotemporal dementia (FTD). Two major pathologies stemming from the hexanucleotide RNA expansions (HREs) have been identified in postmortem tissue: intracellular RNA foci and repeat-associated non-ATG dependent (RAN) dipeptides, though it is unclear how these and other hallmarks of disease contribute to the pathophysiology of neuronal injury. Here we generated two novel lines of mice that overexpress either 10 or 102 G4C2 repeats mediated by adeno-associated virus (AAV) and characterized relevant pathology and disease-related behavioral phenotypes. Surprisingly, RNA foci pathology is independent of both repeat expansion size, RAN dipeptide formation, and behavioral phenotypes in our AAV-HRE treated mice. Similar levels of intracellular RNA foci developed in both lines of mice, but only mice expressing 102 repeats generated c9-RAN pathology, neuromuscular junction (NMJ) abnormalities, dispersal of the hippocampal CA1, enhanced apoptosis, and deficits in gait and cognition. Neither line of mice, however, showed extensive TAR DNA-binding protein 43 (TDP-43) pathology or neurodegeneration. Our data suggests that RNA foci pathology is not a good predictor of c9-RAN dipeptide formation, and that RAN dipeptides and NMJ dysfunction are drivers of c9-disease pathogenesis. These AAV-mediated models of C9orf72 ALS/FTD will be useful tools for studying disease pathophysiology and developing new therapeutic approaches.

Introduction

Hexanucleotide repeat expansions (HREs) in *C9orf72* are regarded as the most common genetic cause of the progressive neurodegenerative diseases, amyotrophic lateral sclerosis (ALS) and frontotemporal dementia (FTD). ALS primarily affects motor neurons and leads to progressive failure of the neuromuscular system with muscle wasting and paralysis, while frontotemporal dementia (FTD) is caused by the degeneration of neurons in the frontal and temporal lobes leading to cognitive deficits. G_4C_2 repeat expansions in the first intron of *C9orf72* are present in up to 40% of familial ALS and 25 % of familial FTD patients, and are also present in 5-20% of sporadic ALS patients (DeJesus-Hernandez et al., 2011, Renton et al., 2011, Majounie et al., 2012, Renton et al., 2014). Normal healthy *C9orf72* alleles contain between 2-30 repeats, while disease-associated alleles vary in size and can exceed several thousand HREs (DeJesus-Hernandez et al., 2011, Renton et al., 2011). Three different pathological alterations providing clues to the etiology of *C9orf72*-related disease can be found in post-mortem tissue from patients with HREs: first, a reduction in all three mRNA transcripts generated from *C9orf72*, suggesting disease may arise by a loss-of-function mechanism (DeJesus-Hernandez et al., 2011, Belzil et al., 2013, Donnelly et al., 2013); second, formation of intracellular foci by aggregation of RNA expansions; and third, dipeptide repeat proteins (DPRs) which are generated from long expansions via repeat-associated non ATG-dependent (RAN) translation (Cooper-Knock et al., 2014, Schludi et al., 2015).

Recent studies suggest that G_4C_2 expansions and DPRs may induce cell toxicity by sequestration of RNA binding proteins (Cooper-Knock et al., 2014, Lee et al., 2016) and disruption of nucleocytoplasmic transport (Zhang et al., 2015, Freibaum et al., 2015). Models designed to mimic either *C9orf72* haploinsufficiency or toxic gain of function have been developed to identify the combination of factors inducing disease relevant pathology. While

C9orf72 knockout mice display motor and cognitive deficits along with heightened neuroinflammation, these mice do not exhibit any significant neuronal pathology, suggesting that a simple loss-of-function mechanism is unlikely to be the sole cause of C9orf72-linked neurodegeneration (Koppers et al., 2015, O'Rourke et al., 2016). Four different toxic gain-of-function mouse models developed through expression of patient derived *C9orf72* packaged in a bacterial artificial chromosome (BAC) consistently displayed intracellular RNA foci and DPRs in the CNS, though they differed in the generation of ALS/FTD disease phenotypes (Jiang et al., 2016, Liu et al., 2016, O'Rourke et al., 2015, Peters et al., 2015, Chew et al., 2015). There was no consensus between the four models as to what minimum HRE size leads to RNA foci formation, as some transgenic lines failed to form any c9-related pathology with even 100 G_4C_2 repeats (Jiang et al., 2016), while others displayed robust c9RAN expression with as few as 37 repeats (Liu et al., 2016). In contrast to the BAC transgenic mice, which overexpress between 1-7 copies of C9orf72, acute AAV-mediated, actin-promoter-driven expression of $(G_4C_2)^{66}$ in mice recapitulates ALS-like pathology and induces cognitive and behavioral deficits, without any flanking C9orf72 sequence (Chew et al., 2015).

However in these mouse models, several fundamental questions regarding *C9orf72* disease etiology remain unanswered: 1) Does a threshold concentration of RNA foci induce the formation of DPRs *in vivo*; 2) What neuropathological criteria are accurate predictors of behavioral deficits; 3) Which factors alter the balance between ALS and FTD phenotypes? To directly address these issues, we generated mice expressing HREs, utilizing AAV serotype 9 (AAV9) to achieve an acute, widespread expression following cisterna magna delivery in postnatal day 1 (P1) pups. We used two lines of mice expressing HRE expansions (10 and 102 repeats) to examine the effects of repeat length on disease etiology. We show that both AAV-$(G_4C_2)^{10}$ and AAV-$(G_4C_2)^{102}$ repeats lead to the formation of a similar number of intranuclear

RNA foci in the CNS *in vivo*, but only $(G_4C_2)^{102}$ transgenic mice generate DPRs, have Purkinje cell apoptosis, exhibit neuromuscular junction pathology, and display gait and cognitive deficits.

Materials and Methods

Antibodies and Reagents

Rabbit anti-AAV VP1, VP2, VP3 (1:800, #03-61084, American Res Prod, USA), rabbit anti-NeuN (1:500, Cell Signalling (USA)- clone D3S3I), rabbit anti-GFAP (1:2000, Dako - Z0334), Rabbit anti-TDP-43 (1:500, Proteintech - catalog #18-280-1-AP), mouse anti-Calbindin (1:1000, Sigma C9848), mouse anti-p62 lck ligand (1:1000, BD Biosciences, clone 3,610833), rabbit anti-α-tubulin (1:5000, Abcam, cat #4074), rabbit-cleaved-caspase 3 (1:1000, Cell Signalling #9661), mouse anti-cleaved PARP (1:250, Cell Signalling #9548), mouse anti-GAPDH (1:5000, Millipore), mouse anti-poly(Glycine-Alanine (GA), 1:500 for western blot; 1:5000 for ICC, clone 5F2 (Mackenzie et al., 2013) kindly provided by Dieter Edbauer) were used at the dilutions listed above.

Cell lines and culture

HEK 293T cells (Sigma) were maintained in growth media (GM) consisting of Dulbecco's modified Eagle's medium (DMEM, D5796, Sigma (USA)) supplemented with 10% foetal bovine serum (Sigma, USA), penicillin (100U/ml), and streptomycin (100U/ml) at 37°C and 5% CO_2, and checked routinely for mycoplasma and authenticated.

Generation of Repeat Expansion Constructs

Sense (TCGAC $(G_4C_2)^{10}$) and antisense (ACGT$(G_4C_2)^{10}$) oligonucleotides (Sigma-Aldrich) with SalI/XhoI overhangs were annealed by denaturing at 95ºC for 5 min and cooling at 0.5ºC/min to 25ºC. The dsDNA $(G_4C_2)^{10}$ was ligated into SalI and XhoI digested pcDNA6.2-GW/EmGFP-miR (Invitrogen) to generate pcDNA6.2-GW-$(G_4C_2)^{10}$. Further $(G_4C_2)^n$ repeats where *n* varied between 10-17 repeats were subcloned into the XhoI site to generate the longer pcDNA6.2-$(G_4C_2)^{102}$ construct. The $(G_4C_2)^{10}$ and $(G_4C_2)^{102}$ constructs were subsequently sub-

cloned into a pAV2-CMV (cytomegalovirus) plasmid and authenticity was confirmed by sequencing. Transformations of plasmids containing the $(G_4C_2)^n$ repeat constructs were performed using recombination-deficient β-10 E.coli (NEB) to minimise any rearrangements.

Large scale scAAV9 production

Sixty 15 cm plates containing HEK293 cells at 80% confluence were transfected using polyethylenimine (MW ~ 25K) with a mixture of three plasmids required to generate an infectious scAAV9 viral particle: (1) A plasmid providing helper genes isolated from adenovirus that enhance viral infectivity (pHelper); (2) An ITR-containing plasmid carrying the gene of interest (pAV2-CMV-(G4C2)n; we used the pAV2-CMV-GFP consisting of two ITRs in a truncated genome that resulted in a self-complementary AAV9 (scAAV9), as described by others (McCarty et al., 2001)); (3) A plasmid that carries the AAV Rep-Cap proteins (pAAV2/9). Each 15cm plate was transfected with a total of 40µg of DNA comprised of a 2:1:1 molar ratio of pHelper: pAV2-CMV-$(G_4C_2)^n$: pAAV2/9. Four days after transfection, the AAV enriched media was collected, incubated at 37°C for 2 hours with 3,750 units of benzonase-nuclease (Sigma, USA), filtered through a 0.22 µm filter, and concentrated to a volume of 1ml using Amicon spin filter units (Millipore, USA). The virus was then washed with 50 ml of phosphate buffered saline (PBS, pH 7.3) in the same Amicon spin filter units, and concentrated to a final volume of 0.5 ml. The viral sample volume was expanded to 14ml with PBS and separated through a discontinuous iodixanol (D1556, Sigma, USA) gradient (4ml of 54%, 9 ml of 40%, 9 ml of 25%, 5 ml of 15%), and centrifuged at 69,000 rpm for 1.5 hours at 18°C. Phenol red was added to the 54% and 25% iodixanol layers to help with identifying the virus enriched layer. The purified virus was found as a white layer between the 54% and 40% iodixanol gradient and subsequently removed in 0.5ml fractions using a syringe, with 10µl of each fraction mixed at an equal ratio with 2X reducing sample SDS-PAGE buffer, heated to

75°C for 20 minutes, separated on a 4-20% precast TGX mini-gel (Biorad, USA), and stained with Sypro-Ruby according to the manufacturer's protocol (Life Techologies, USA). Fractions that showed a pure virus composed solely of the VP1, VP2 and VP3 bands were combined, and washed against 5 full volumes (15ml each) of PBS with an Amicon spin filter, before collecting in a final volume of between 300-500µl.

Quantitative PCR to measure viral titres

Viral titres were determined with the Quantifast SyBR Green PCR Kit (Qiagen, Cat 204054) on a BioRad CFX96 thermal cycler, following the manufacturer's instructions. The number of copies in three dilutions of a purified AAV9 virus (1/100, 1/1000, 1/10,000) were compared to a standard curve generated by serial dilutions of a linearized pAV2-CMV-$(G_4C_2)^n$ vector. Primers used to quantify viral genomes were (Poly A, Forward: 5'-ATT TTA TGT TTC AGG TTC AGG GGG AGG TG-3'), (PolyA, Reverse: 5'-GCG CAG AGA GGG AGT GGA CTA GT-3').

RNA Fluorescent in-situ hybridization (FISH)

RNA FISH was performed as described previously (Cooper-Knock et al., 2014) with a few modifications. Briefly, a 5' TYE-563-labelled LNA (16-mer fluorescent)-incorporated DNA probe was used against the sense RNA hexanucleotide repeat (Exiqon, Inc., batch number 607323). Coronal brain sections (20 µm) directly cut onto slides were air dried, and then incubated in ice cold acetone for 10 minutes before washing in PBS. Slides were blocked with a hybridization solution [50% formamide, 2× saline sodium citrate (SSC), 100 mg/ml dextran sulphate, 50 mM sodium phosphate pH 7.0] for 1 h at 66°C and then incubated with 400 ng/ml of denatured probe in hybridization solution overnight at 66°C. After hybridization, slides were

washed once in 2×SSC/0.1% Tween-20 at room temperature and three times in 0.1× SSC at 65°C and counterstained with Hoechst 33342. All solutions were made with DEPC-treated water.

Generation of AAV9-mediated mouse model

Mice were kept in a 12-hour dark/12-hour light cycle, with free access to food and water and a standardized room temperature, based on the UK Home Office Code of practice for the housing and care of animals used in scientific Act 1986. All *in vivo* experiments carried out in this study were performed according to the Animal (Scientific Procedures) Act 1986, under the Project License 40/3739, and were approved by the University of Sheffield Ethical Review Sub-Committee and the UK Animal Procedures Committee (London, UK).

Viruses ($4.5x10^{10}$ vg; scAAV9-CMV-$(G_4C_2)^{10}$ or scAAV9-CMV- $(G_4C_2)^{102}$) were injected into the cerebrospinal fluid (CSF) of postnatal 1 (P1) male and female C57BL/6J wild-type mice, via the cisterna magna, under general anaesthesia. Pups from the same breeding pair were allocated randomly to the experimental groups. Viral delivery was carried out following the protocol described in previously (Lukashchuk et al., 2016). Briefly, pups were anaesthetized in an induction chamber using 5% isoflurane and oxygen at 3 L/min before placing the animal over a red transilluminator in the prone position. Viruses were loaded in a Hamilton syringe attached to a peristaltic pump and injected into the cisterna magna, using a stereotaxic apparatus, at a flow rate of 1 µl/min to a maximum volume of 5 µl. Anaesthesia was maintained with 2% isoflurane and oxygen at 0.3 L/min during the injection.

Immunohistochemistry

Twelve months after injection, animals were sacrificed under terminal anaesthesia and transcardially perfused using a solution of PBS-heparin followed by 4% paraformaldehyde (PFA) in PBS. Brain and spinal cords were harvested and further post-fixed overnight in 4% PFA. After fixation, tissue was washed with PBS, cryoprotected in 30% of sucrose at 4°C, embedded in OCT (Cell Path®), and snap frozen in liquid nitrogen. Brains and spinal cords were cut in 20 μm thick coronal sections on a cryostat (Leica), placed directly onto silane treated slides, and then air dried. Sections were incubated with gentle agitation for 2 hours at room temperature in blocking buffer (PBS with 5% normal goat serum, 3% BSA and 0.2% Triton-X-100) before incubating overnight at 4°C with the appropriate antibody diluted in PBS with 3% BSA. Following three washes with PBS, sections were incubated with an appropriate alexa fluorophore conjugated secondary antibody (1:1000; Invitrogen, CA) for 1 hour at room temperature, counterstained with Hoechst 33342 and mounted onto slides with Fluoromount (Sigma). For visualizing DPR pathology, slides were immersed in
sodium citrate buffer (10mM Sodium Citrate, 0.05% Tween 20, pH 6.0) for 30 minutes at 60°C before the blocking step.

Neuromuscular junction (NMJ) pathology

NMJ pathology was assessed on whole-mount immunohistochemically-labelled preparations of hindpaw lumbrical muscles from 1 year old mice, as described previously (Powis et al., 2016, Wishart et al., 2014). Images were captured using a Nikon A1R confocal system combined with a Ti:E inverted microscope (×60 objective). Individual NMJs were assessed and abnormalities quantified, by eye, for evidence of neuromuscular pathology (presence of axonal blebbing/thinning or abnormal neurofilament accumulations in distal motor axons and/or motor nerve terminals). NMJ analysis was performed by investigators blinded to the treatment group.

Quantitative Fluorescence Imaging

To assess the effect of CG repeats on the postsynaptic receptor density (marker of synapses), muscle cells were labeled with a saturating dose of fluorescent BTX (5 ug/ml, ~1 hour) and images of NMJs were collected using IPLAB software as described previously (Akaaboune et al., 1999, Martinez-Pena et al., 2015). The fluorescence intensity of labeled AChR was analyzed with algorithms for Matlab (The Mathworks). Background fluorescence was determined by manual selection of a boundary region around the each NMJ and subtracting it from the original image, and the mean of the total fluorescence intensity (which corresponds to total fluorescence of that synapse divided by the area of that given synapse) was measured (Turney et al., 1996, Akaaboune et al., 1999, Martinez-Pena et al., 2015). All calculations of fluorescent intensities were made by investigators blinded to the mouse genotypes.

Immunoblotting

Adult mice were sacrificed using an overdose of sodium pentobarbitol, and brains were rapidly dissected and snap frozen with liquid nitrogen. Brains were then homogenised in RIPA buffer using a glass dounce homogenizer (150mM NaCl, 50mM Tris pH8, 0.5% sodium deoxycholate, 0.1% sodium dodecyl sulphate (SDS), 1% NP-40 supplemented with 1X EDTA-free protease inhibitor cocktail (Roche)) for 30 minutes on ice and centrifuged at 17,000 g at 4°C for 10 minutes. Supernatant was then collected as a cytoplasmic fraction and used to examine p62 reactivity. To examine poly (GA) DPRs, the membrane enriched pellet was further solubilized in a buffer containing 1% Triton-X-100 and 0.5M NaCl in 10mM Tris-HCl (pH 7.4) for 45 minutes at 4°C with constant agitation and centrifuged at 17,000g at 4°C for 10 minutes. Supernatant was collected as the triton-soluble fraction and the pellet was re-suspended in a buffer containing 2% SDS in 10mM Tris-HCl (pH 7.4) and stored as the Triton insoluble fraction. Protein lysates were mixed with a 4X Laemmli buffer with 5% β-

mercaptoethanol, heated to 95°C for 5 minutes, separated with a 10% SDS-PAGE and transferred onto a PVDF membrane (Millipore). Membranes were blocked with either 5% BSA or 5% nonfat dry milk in TBS with 0.05% Tween (TBST) for 30 minutes, before incubating at 4°C overnight with agitation with the appropriate antibody diluted in 5% BSA in TBST. Following three washes in TBST for 10 minutes each, membranes were incubated at room temperature with mild agitation with an appropriate secondary HRP antibody (Sigma Aldrich, 1:5000) diluted in 5% BSA in TBST, washed three times with TBST for 10 minutes each, and developed with enhanced chemiluminescent substrate (Amersham-Pharmacia Biotech, USA).

Mouse Behavioural Tests

All mouse behavioural experiments were performed with the experimenter blind to the mouse cohort groups.

Open Field

The open field was a 60cm x 40cm x 25cm semi-transparent plastic box with a grid of 3x5 squares drawn on the underside of the box with black paint. Open field activity was measured in a room with minimal light for 10 minutes with the number of squares crossed recorded. A square crossing was defined as the passage of all four mouse paws over one of the boundaries of a square.

Object Recognition

Mice were tested for their ability to remember novel objects using a paradigm described by others (Leger et al., 2013). Briefly, on day 1 mice were habituated in a rectangular 60cm x

40cm x 25cm open field for three minutes. On the second day, mice were placed in the same box with two identical objects, and allowed to explore until a total of 20 seconds of exploration between the two objects had elapsed. Exploration was defined as mice actually sniffing, biting, touching with paws or examining the object. On the third day, one of the objects was replaced with a novel object, and the time measured at each object was recorded until a total of 20 seconds had elapsed. To make sure that the objects were interesting enough to entice mice to explore them, the first object was a standard red capped 75cm^2 tissue culture flask (Sigma, C7231) filled with a layer of purple dye treated agarose, while the second object was a stack of red slide boxes taped together.

Gait analysis

To analyse the gait pattern, 6 and 12 month old mice were placed on the Catwalk XT (Noldus®, Netherlands), where they had to traverse a narrow chamber in the dark. Their footprints were automatically recorded with the Catwalk 7.1 software from Noldus®. Six runs were performed per animal and the three best (chosen for mice walking along the chamber path as opposed to repeatedly stopping) were selected for analysis. All results are expressed as the average of 3 runs ± SEM. The following parameters were measured and defined as:

Stand. The time the paws spends in contact with the Catwalk surface.

Base of support (BOS). Distance between either the front or hind paws.

Diagonal support. Time spent on the Catwalk surface by a front paw and its opposing hind paw simultaneously (Right front paw – rear hind paw).

Three support. Time spent on the Catwalk surface by three paws at the same time to support animal.

Swing. Time between two consecutive placements in which the paw is not in contact with the Catwalk surface.

Swing speed. This parameter is calculated by dividing the stride length by the swing phase duration.

Hind limb splay

Twelve month old mice were suspended by the tail and the splay defects were observed and scored for right and left hind-limbs by using the following scale: 0:normal splay; 1:mild defect; 2: moderate defect; 3: strong defect; 4: paralysed as previously described (Mead et al., 2011) The results show the average of each group ± SEM.

Rotarod

Performance on the rotarod (Ugo Basile 7650) was assessed every 2 weeks, twice per day, beginning 2 months after injection. Mice were initially trained for 3 consecutive days before the first trial. The rotarod was set to accelerate from 3 to 37 rpm in 300 seconds and the maximum time spent on the rotarod in a single trial out of two trials tested was recorded.

Statistical Analysis

Results are shown as mean ± standard error (S.E.M.). Student's unpaired *t*-test with a Welch's correction for two group comparisons was used to assess differences between HRE-10 and HRE-102 mice. For comparisons between three groups (PBS injected, HRE-10 and HRE-102 mice), a one-way analysis of variance (ANOVA) was used with Tukey's multiple comparison post-hoc test when $p < 0.05$. For assessing the effects of age on the gait and activity in each mouse cohort, we used a two-way ANOVA with a Sidak's test for multiple comparisons when

$p<0.05$. No animals were excluded from any of the statistical analysis, and the cohorts were a mixture of male and female mice. For behavioural analysis, investigators were blinded to the mice being tested. All cell counts and RNA foci analysis were made by investigators blinded to the mouse genotypes. For all tests, a *P*-value < 0.05 was taken as statistically significant, and Graphpad Prism 6 was used for all statistical analyses.

Results

Injection of AAV9-$(G_4C_2)^{10}$ and AAV9-$(G_4C_2)^{102}$ generate intranuclear RNA foci in vivo

In these studies, we used self-complementary AAV9, due to its enhanced CNS transduction efficiency compared to single stranded AAV9 (McCarty et al., 2001) and its ability to achieve transduction in multiple regions of the mouse brain (Lukashchuk et al., 2016). To generate mice expressing HREs, we first constructed two separate AAV9 vectors containing either 10 or 102 HREs (Figure 1A). The AAV9-$(G_4C_2)^{102}$ (referred to as HRE-102) construct was made by ligating between 10-17 HREs separated by a short TCGAG linker sequence, which results in mixed dipeptide repeat proteins. The advantages to using this approach are: firstly, the interruptions stabilized the sequence, reducing the risk of DNA rearrangements between the flanking inverted terminal repeats (ITRs) of the AAV; secondly, our HRE-102 did not have internal stop codons, which allowed us to test whether c9-pathological hallmarks, such as DPRs and TDP-43 aggregation, still persist in the presence of interrupted repeat sequences.

Mice expressing repeat expansions were generated by delivering AAV9-HREs to early postnatal (P1) mice via the cisterna magna, which resulted in widespread transduction of the adult mouse brain as described in our previous work (Lukashchuk et al., 2016). Twelve months after AAV9 delivery, mice were sacrificed and different brain and spinal cord tissue was analysed using RNA fluorescent in situ hybridization (FISH) to see whether intracellular RNA foci were present. We found that the regions with the highest number of RNA foci per area are the brain stem, Purkinje cell layer of the cerebellum, CA1 and hilus of the hippocampus, midbrain, and cortex (Figure 1B-D). RNA foci were also detected in the spinal cord, even though they were less numerous in this region (Figure 1E). Surprisingly, there were no

significant differences in the number of RNA foci between the HRE-10 mice and HRE-102 in any of the regions examined (Figure 1F), suggesting that the formation of RNA foci is independent of the length of the G_4C_2 expansion.

HRE-102 mice exhibit extensive DPR pathology, enhanced p62 expression, and dispersed CA1 neurons

To test whether the AAV9-engineered mouse model develop other pathological hallmarks of ALS/FTD such as c9RAN protein aggregates, TDP-43 inclusions, and neuronal loss, we used a poly-GA antibody (Mackenzie et al., 2013) to probe for glycine-alanine rich DPRs in mouse brains. As shown in Figure 2, we detected either a homogenous nuclear expression (arrow) or an intense, discrete staining (arrowhead) within and outside of the nucleus (Figure 2A). These type of poly-GA pathology (diffuse or aggregate staining) which were most widely distributed in the cerebellum and brain stem, were visible only in HRE-102 (67%, n=6) treated mice, and absent in HRE-10 expressing (0%, n=6) mice. Analysis of triton-insoluble and soluble cerebellar/brain stem lysates isolated from a different group of HRE-10 and HRE-102 mice identified several different sized poly-GA peptides ranging from 25-63 kilodaltons in both triton-soluble and insoluble fractions solely in a subset of HRE-102 mice (Figure 2A-B). Additionally, the expression of p62, a marker of c9RAN pathology (Mori et al., 2013a, Mori et al., 2013b, Schludi et al., 2015), was enhanced in HRE-102 mice (Figure 2C).

Next, we examined the expression of cleaved-caspase 3 and cleaved poly (ADP-ribose) polymerase (PARP) to see whether there was evidence of cells undergoing apoptosis. We focused our analysis on the cerebellum, due to the heightened DPR and p62 expression we observed in the HRE-102 mice (Figure 2A-C) that have been correlated to cell toxicity (Lee et al., 2016, Lopez-Gonzalez et al., 2016, Tran et al., 2015). As shown in Figures 2D-F, we found

that cleaved PARP in cerebellar purkinje cells and cleaved caspase-3 expression in the cerebellum were significantly increased in HRE-102 mice, indicating that that these areas were in the early stages of cell death. Interestingly, despite the presence of RNA foci and c9RAN pathology, neither astrogliosis (Figure S1) nor neurodegeneration in the cerebellum (Figure S2C-D) were observed. This absence of repeat-length dependent neurodegeneration was also observed in other such as the cortex (Figure S2A-B), spinal cord (Figure S2E-F) and hippocampus (Figure 2D-E), though there was a significant dispersal in the CA1 (Figure 2G-H) that is characteristic of *reeler* mutant mice (Howell et al., 1997, Trommsdorff et al., 1999). Additionally, although we were able to detect infrequent TDP-43 clusters (Figure S3A-B) in the cerebellum, cortex, midbrain and hippocampus of HRE-10 and HRE-102, there was no significant difference between mouse groups with respect to TDP-43 pathology. In contrast to the largely nuclear TDP-43 pathology reported by Chew et al (2015), the majority of TDP-43 aggregates in both groups of AAV-HRE injected mice were either at the perinuclear region or in the cytoplasm (Figure S3C).

HRE-102 mice develop disease-related neuromuscular junction (NMJ) pathology

In the absence of significant loss of neuronal cell bodies in the CNS in both mouse cohorts and since NMJ pathology is present in several different mouse models of ALS (Iguchi et al., 2013, Frey et al., 2000, Murray et al., 2010, Bennett et al., 2014), we asked whether peripheral neuromuscular junctions were altered in the HRE-102 expressing mice. To do this, muscles from twelve-month old mice were doubly labelled with an anti-neurofilament antibody to label nerve terminals and fluorescent bungarotoxin to label acetylcholine receptors (AChRs), and NMJs were imaged with a confocal microscope. A close inspection of NMJs revealed a significant increase in pathological NMJs in HRE-102 mice, defined as having abnormal pre-

synaptic neurofilament accumulations and/or nerve terminal blebbings (Figure 3A,B), indicating that the NMJ may be an early target of c9-related toxicity. It well established that the density of postsynaptic AChR is significantly reduced in mouse models of motor neurons disease and myasthenia gravis (Losen et al., 2005, Kong et al., 2009). Here we asked whether the density of AChR at NMJs of HRE-102 mice is also altered. AChRs were labeled with BTX-594 and the density of AChR at NMJs of HRE-102, HRE-10 and PBS were compared (Figure 3C-D). The total fluorescence of AChRs (which measured fluorescence of a synapse per area of the synapse) was decreased by 20% in muscles expressing HRE-102 compared with NMJs of PBS injected mice. These results indicate that HRE-102 expression reduces the density of AChRs at postsynaptic sites. Collectively, HRE-102 mice exhibit a loss in NMJ integrity at 12 months of age that is consistent with the early stages of motor neuron degeneration.

HRE-102 mice have progressive gait and behavioural deficits

To assess whether the c9RAN and NMJ pathology have any consequences on mouse behaviour, we analysed motor and cognitive tasks. We used a Catwalk system to examine different parameters measuring motor coordination and gait in ambulatory mice, and found that HRE-102 mice had gait abnormalities, with significantly irregular gait patterns compared to HRE-10 mice in the stand, base of support (BOS), diagonal support and three support parameters (Figure 4A). When we assessed the hindlimb splay in the two cohorts (HRE-10 and HRE-102), we found that there was a significant defect in the right hindlimb in the HRE-102 mice (Figure 4B). These deficits did not appear to affect the exploratory activity of the mice as HRE-102 mice were not significantly different to HRE-10 mice in the open field at 12 months of age (Figure 4C). When we analyzed data between 6 and 12 months of age from several of the same tasks, we noted that most of the gait parameters including ones for measuring stride

irregularities (stand, swing, and swing speed) in addition to activity in the open field showed significant deterioration with age in the HRE-102 mice (Figure S4A-D), demonstrating that the behavioural impairments in HRE-102 mice were progressive. There were, however, no differences between groups in the accelerating rotarod over the ten months of testing (Figure S4E). We next used the object recognition paradigm to determine whether the HRE-102 mice had any cognitive deficits which could correlate with the CA1 dispersal demonstrated in Figure 2D. This behavioural task exploits the innate interest of mice to explore a novel object by forcing mice to discriminate between a novel object and an object previously explored. Both sets of mice explored two novel objects without any significant difference in the familiarization phase (Figure 4D), but only HRE-102 mice were unable to discriminate between a novel object and one they had previously explored, indicating the presence of a memory deficit.

Discussion

Current mouse models of C9orf72 ALS/FTD have supported a toxic gain of function mechanism by which long G_4C_2 hexanucleotide RNA expansions (HREs) induce the formation of intracellular RNA foci and RAN protein aggregates leading to toxicity and behavioural dysfunction. One of several issues which remains unclear, however, is the minimum pathogenic size of the repeats and specific mixture of factors necessary for generating disease. Here we have directly addressed this important question by developing a new model of C9orf72 ALS/FTD utilizing AAV9 to express either 10 or 102 interrupted G_4C_2 repeat expansions, and demonstrate that while both lines of mice have similar numbers of RNA foci dispersed through the brain, only AAV-HRE-102 mice generate c9RAN pathology, exhibit NMJ pathology, hippocampal CA1 dispersion, early markers of apoptosis, and display gait and cognitive deficits.

To date, four independent mouse models expressing either a full length or truncated human C9orf72 have been generated with hundreds of HREs along with an AAV-mediated model expressing a shorter (66) number of HREs. All of these mouse models have detectable RNA foci and c9RAN aggregates in the brain, though the minimum size necessary to induce RNA foci formation differs widely. Expression of a full length C9orf72 bacterial artificial chromosome (BAC) transgene in mice was unable to induce RNA foci formation with even 36-37 HREs (Liu et al., 2016, O'Rourke et al., 2015), and in mice expressing truncated C9orf72, expression of even 100 G_4C_2 expansions yield limited RNA foci (Jiang et al., 2016). In contrast, AAV mediated expression of 66 HREs resulted in mice displaying significant ALS/FTD pathology (Chew et al., 2015). The likely major difference between model systems is that AAV based models can utilize a strong promoter to drive expression such as the actin

promoter used by Chew et al. (2015) or the cytomegalovirus (CMV) promoter we have used in the present study. In the AAV C9orf72 model described by Chew et al. (2015), expression of only two HREs failed to generate any RNA foci or DPRs. We chose a higher minimum expansion length of 10 HREs to get a better gauge of whether the expression of RNA foci and RAN translated DPRs were linked, since we had detected RNA foci in both cell lines and primary neurons transduced with HRE-10 (unpublished observations). Surprisingly, our mouse models expressing HRE-10 and HRE-102 yield similar numbers of RNA foci in the CNS (Figure 1F), and we therefore conclude that RNA foci density is not dependent on the length of an expansion repeat once a minimum threshold has been crossed.

Although other groups have shown that crossing a minimum HRE threshold may be necessary to induce DPR formation (Mizielinska et al., 2014, Zu et al., 2011), there is a report of BAC C9 transgenic mice overexpressing 36/37 HREs and forming poly-GA aggregates without RNA foci formation (Liu et al., 2016). There remains the possibility, therefore, that RNA foci and DPRs arise independently of each other. Our data support a relationship between expansion repeat length and DPR formation since only the HRE-102 mice expressed DPRs (Figure 2A-B) as well as increased p62 staining (Figure 2C), which frequently co-localizes with poly-GA DPRs (Schludi et al., 2015). The presence of DPRs in our HRE-102 mice also indicates that the interruptions we introduced between every 10-17 GGGGCC repeats do not prevent protein expression, unlike the interrupted HREs expressed in *Drosophila melanogaster* (Mizielinska et al., 2014). This is probably due to the absence of stop codons within the repeat expansions in our AAV construct, demonstrating that a pure $(G_4C_2)^n$ sequence is not necessarily required to induce RAN translation and the formation of either diffuse protein expression or aggregates. There is a growing consensus that DPR expression is toxic to cells, and a key factor in C9-related disease (Zhang et al., 2015, Lee et al., 2016, Mizielinska et al., 2014), although two of

the BAC transgenic C9-mouse models generate DPRs without any concomitant neurodegeneration or behavioral dysfunction (Peters et al., 2015, O'Rourke et al., 2015). Our data support a link between DPRs and toxicity; HRE-102 mice express DPRs and have progressive gait, activity and cognitive deficits along with changes in the integrity of the NMJ that are absent in HRE-10 mice. Additionally, the HRE-102 mice show early signs of apoptosis including an increased expression of cleaved caspase-3 (Figure 2F) and cleaved PARP expression (Figure 2G-H) in the cerebellum, which had the highest concentration of DPRs. In contrast to the largely nuclear DPRs generated in mice expressing HRE-66 with AAV9 (Chew et al., 2015), our AAV9 mediated HRE-102 mice primarily showed discrete DPR aggregates in the cytoplasm (Figure 2A), similar to several human C9orf72 BAC transgenic models (Jiang et al., 2016, O'Rourke et al., 2015, Peters et al., 2015) and observed in C9ALS/FTD patients (Mori et al., 2013a, Mori et al., 2013b, Schludi et al., 2015). Our data therefore supports a repeat-length dependent change in the formation of DPRs and suggest that even with a strong constitutive promoter, there needs to be more than 66 HREs to detect DPRs in the cytoplasm.

As HREs in *C9orf72* are a major cause of FTD, and progressive deficits in spatial learning and memory and have been reported in C9orf72 BAC transgenic mice expressing 450 repeats linked to mild neuronal loss in the dentate gyrus and hippocampal CA1 (Jiang et al., 2016), we carefully examined hippocampal pathology in the AAV-mediated mouse models since the HRE-102 mice failed to discriminate between familiar and novel objects, demonstrating the presence of a cognitive deficit (Figure 4D). Previously, DPRs in the hippocampal CA1 of patients with C9-repeats have been reported (Pletnikova et al., 2014), but while we did not detect DPRs in the hippocampus, we did observe a dispersal of the CA1 (Figure 2D-E) in the HRE-102 mice that was reminiscent of the aberrant neuronal migration phenotype of Reeler/Disabled-1 mouse mutants that occurs during early development (Trommsdorff et al.,

1999, Howell et al., 1997). Interestingly knockdown of Reelin, the glycoprotein absent in Reeler mutant mice, impairs rats in the object recognition task, while Reelin overexpression can rescue deficits in the object recognition task in mouse models of Alzheimer's disease (Brosda et al., 2011, Pujadas et al., 2014). Further analysis will be necessary to determine whether any link between Reelin and C9orf72 exists.

In summary, these data support a repeat-expansion length dependent gain of toxicity, with c9RAN formation being the likely driver of pathogenesis as the gait, motor and cognitive deficits precede any major TDP-43 pathology. Our mouse models, generated through AAV-mediated expression of HREs, have allowed us to uncouple the relationship between RNA foci pathology, DPR formation and repeat expansion length. RNA foci pathology is not dependent on the length of the repeat expansion, and appears to be independent of both DPR formation as well as disease relevant behavioral phenotypes in our AAV-HRE expressing mice. In our mouse model expressing 102 HREs, the structural changes in the NMJ may correspond to the observed gait abnormalities, and changes in CA1 integrity may be linked to cognitive deficits, though further evaluation in the future will be necessary to assess this. Our studies establish a new mouse model generated by utilizing AAV9 to achieve widespread expression of HREs in mice, which will be useful for identifying therapeutic strategies that ameliorate DPR toxicity.

Acknowledgements

We thank Dieter Edbauer for the use of the poly-GA antibody and Joseph Scarrot for critical reading of the manuscript. scAAV and pAAV2/9 plasmids were gifts from J. Gray and J. Wilson, respectively. The authors have declared that no conflict of interest exists

Funding

This work was supported by the European Research Council grant (ERC Advanced Award no. 294745) to MA. M.A. is also supported by MRC DPFS Award (129016). S.H.M, K.E.A.L., J.C., P.M., I.C. and CW were supported by ERC Advanced Award (294745). CW is half funded by the Wellcome Trust Investigator Award (103844) to S.F.E-K. P.J.S is supported as an NIHR Senior Investigator and by the Motor Neurone Disease Association (grant Apr16/846-791) and the Medical Research Council (MRC) (grant MR/M010864/1 in collaboration with Professor Jun Xu (Projects of International Cooperation and Exchanges NSFC:81261130318) at Tongji University in China). S.F.E-K is funded by a Wellcome Trust Investigator Award (103844), a Lister Institute of Preventative Medicine Fellowship, and a European Union British Council award. T.H.G. was supported by the UK SMA Research Consortium (SMA Trust).

Figure Legends

Figure 1. AAV9-HREs can generate RNA foci in the mouse CNS. (A) Two different HREs were designed and subcloned into AAV9 vectors with the $(G_4C_2)^{102}$ expansions constructed by a mixture of $(G_4C_2)^{10\text{-}17}$ oligonucleotides with an intervening linker sequence. (B-F) RNA fluorescent in situ hybridization was used to detect RNA foci, which were abundant in the (B) hippocampus (HC), (C) cortex (CTX), (D) cerebellum (CB) and sparse in the (E) spinal cord (SC, *motor neuron). (F) There were no significant differences in the number of foci detected per mm^2 in either the HC (n=3 for each, p=0.28), CTX (n=3 for each, p=0.43), or CB (n=6 for each, p=0.73) between HRE-10 and HRE-102 mice as assessed using an unpaired two-tailed Student's t-test with Welch's correction for each region. Scale bar is 10μm. Nuclei stained blue.

Figure 2. Dipeptide protein repeat (DPR) pathology, hippocampal CA1 dispersal, and upregulation of cell death markers are observed in HRE-102 mice. (A) Cytoplasmic and nuclear DPRs adopt several morphologies in a subset of HRE-102 mice using a poly-(GA) antibody in cerebellar tissue. (B) Immunoblots of cerebellar lysates show that both triton soluble and triton insoluble proteins contain GA-rich DPRs in HRE-102 mice, and were never observed in HRE-10 mice. (C) HRE-102 mice show an increased p62 expression compared to HRE-10 mice in cerebellar tissue; arrowhead shows 60 kD isoform that was consistently absent in HRE-10 brains. (D-E) A significant number of Purkinje cells in the cerebellum of HRE-102 mice show signs of early apoptosis reflected by cleaved PARP immunoreactivity (n=4 for both, p=0.046). (F) Enhanced cleaved-caspase-3 expression is observed in cerebellar lysates from HRE-102 mice. (G-H) There were no differences in the number of neurons as determined by NeuN staining in the dentate gyrus (DG, HRE-10 (n=4), HRE-100 (n=6); p=0.66) or CA3 (HRE-10 (n=4), HRE-100 (n=6); p=0.69) in the hippocampus between HRE-10 and HRE-102, but there was a significant dispersal of CA1 neurons in HRE-102 mice (HRE-10 (n=4), HRE-

100 (n=6); p=0.046). Nuclei stained blue. All comparisons were made with an unpaired two-tailed Student's t-test with Welch's correction; mean ± SEM. Scale bar: (A): 10 μm, (D): 25 μm, (G): 10 μm

Figure 3. Neuromuscular junction (NMJ) defects are present in the HRE-102 mice. (A-B) Abnormal neurofilament accumulation and nerve terminal blebbings (arrows) were prominent in HRE-102 mice (PBS:n=3, HRE-10:n=4, HRE-102:n=4; n=individual muscles per genotype; ($F(2,8)=6.47$, *p=0.02, post-hoc Tukey: HRE-10 vs PBS (p=0.19); HRE-10 vs HRE-102 (p=0.23); HRE-102 vs PBS (p=0.02)); scale bar 30 μm. (C-D) HRE-102 mice have a significant decrease in acetylcholine receptor density compared to PBS injected controls ($F(2,7)=10.79$, **p=0.007, post-hoc Tukey: HRE-10 vs PBS (p=0.16); HRE-10 vs HRE-102 (p=0.056); HRE-102 vs PBS (p=0.006)). The fluorescence intensity (total fluorescence of that synapse divided by the area of that given synapse) of a saturating dose of α-bungarotoxin-alexa fluor 594 was measured and normalized to PBS controls. All comparisons were made with a one-way ANOVA and post-hoc Tukey for comparisons between groups; mean ± SEM.

Figure 4. Gait and cognitive deficits observed in HRE-102 mice are absent in HRE-10 mice in 12 month old mice. (A) Gait abnormalities such as the front and hind stand index, the hind base of support (BOS), the diagonal support and the three-legged support were observed using a Catwalk system in HRE-102 mice (HRE-10 (n=11), HRE-100 (n=13) for each; front stand:*p=0.04, hind stand:*p=0.04; front BOS:p=0.19, hind BOS:*p=0.02; diagonal support:*p=0.01, three-legged support:**p=0.006). (B) HRE-102 mice (n=13) had a moderate splay in the right (*p=0.04) but not left (p=0.59) hindlimb compared to HRE-10 mice (n=11). (C) There were no significant differences in activity (p=0.15) between HRE-10 (n=11) and HRE-102 (n=13) in the open field. (D) An object recognition test identified a cognitive deficit in HRE-102 mice (n=13) as they failed to discriminate in the testing phase (HRE-102:familiarization phase: p=0.43, testing phase: p=0.09) between a novel object and an object

previously explored in the familiarization phase unlike HRE-10 mice (n=11, familiarization phase:p=0.57, testing phase:*p=0.02). All comparisons were made with an unpaired two-tailed Student's t-test with Welch's correction; mean ± SEM.

Figure S1. No differences in astrogliosis between HRE-10 and HRE-102 mice. GFAP immunoreactivity in twelve-month cerebellar tissue was similar between HRE-10 and HRE-102 mice (n=3 for each; p=0.79, unpaired two-tailed Student's t-test; mean ± SEM).

Figure S2. No evidence of loss of neuronal cell bodies in the cortex or cerebellum of HRE-102 mice. (A) NeuN immunoreactivity in the cortex in twelve-month cortical tissue was not significantly different (B) between repeat expansion mice (n=5 for each; p=0.15, unpaired two-tailed Student's t-test with Welch's correction; mean ± SEM). (C) Calbindin immunoreactivity, used to label Purkinje cells in the cerebellum, was not significantly different (D) between HRE-10 and HRE-102 mice (n=5 for each; p=0.37, unpaired two-tailed Student's t-test with Welch's correction; mean ± SEM). (E) Nissl staining of spinal cord sections show that there are no significant differences (F) between HRE-10 and HRE-102 in the number of motor neurons in the spinal cord (n=3 for each; p=0.87, unpaired two-tailed Student's t-test with Welch's correction; mean ± SEM). Scale bar for (A): 10μm, (C): 20μm, (E): 20 μm.

Figure S3. No differences in presence of TDP-43 aggregates between HRE-10 and HRE-102 mice. (A) Infrequent TDP-43 aggregates were identified in brain tissue in (B) multiple regions, though there were no significant differences detected between the HRE-10 and HRE-102 mice in either the cerebellum (CB, n=3 for each; p=0.89), cortex (CTX, n=6 for each; p=0.48), hippocampus (HC, n=6 for each; p=0.93), or midbrain (MB, n=6 for each; p=0.15). (C) The majority of TDP-43 aggregates were found outside (O, HRE-10:n=6, HRE-102:n=5; p=0.87) the nucleus, with the perinuclear (P, HRE-10:n=6, HRE-102:n=5; p=0.60) and nuclear

(N, HRE-10:n=6, HRE-102:n=5; p=0.52) localization in the minority. An unpaired two-tailed Student's t-test was used to assess data between the two mouse groups for all comparisons. Scale bar for (A): 50μm, (C): 5μm. Nuclei stained blue.

Fig S4. HRE-102 mice show age-related deficits in gait and activity compared to HRE-10 mice. (A-C) Progressive changes in HRE-102 mice in several gait phenotypes such as the front and hind stand index, front and hind swing speed, and front and hind swing are not observed in HRE-10 mice (HRE-10:n=11, HRE-102:n=13; front stand index:[F(1,42)=17.87, ***p=0.0001, post-hoc Sidek: HRE-10 (p=0.29), HRE-102 (p<0.0001)], hind stand index:[F(1,42)=18.63, ****p<0.0001, post-hoc Sidek:HRE-10 (p=0.17), HRE-102 (p=0.0001)], front swing speed:[F(1,42)=10.93, **p=0.002, post-hoc Sidek:HRE-10 (p=0.22), HRE-102 (p=0.007)], hind swing speed:[F(1,42)=9.27, **p=0.004, post-hoc Sidek:HRE-10 (p=0.49), HRE-102 (p=0.004)], front swing:[F(1,42)=15.96, ***p=0.0003, post-hoc Sidek:HRE-10 (p=0.15), HRE-102 (p=0.0007)], hind swing:[F(1,42)=14.46, ***p=0.0005, post-hoc Sidek:HRE-10 (p=0.42), HRE-102 (p=0.0002)]. (D) HRE-102 mice were increasingly hypoactive with age in the open field in contrast to HRE-10 mice (HRE-10:n=10, HRE-102:n=13; front stand index:[F(1,42)=9.69, **p=0.003, post-hoc Sidek: HRE-10 (p=0.36), HRE-102 (p=0.005)]. (E) There were no differences on the accelerating rotarod between HRE-10 and HRE-102 mice [F(22,484)=0.84, p=0.67]; Two-way ANOVA, genotype x age interaction, all data presented as mean ± SEM.

References

AKAABOUNE, M., CULICAN, S. M., TURNEY, S. G. & LICHTMAN, J. W. 1999. Rapid and reversible effects of activity on acetylcholine receptor density at the neuromuscular junction in vivo. *Science,* 286**,** 503-7.

BELZIL, V. V., BAUER, P. O., PRUDENCIO, M., GENDRON, T. F., STETLER, C. T., YAN, I. K., PREGENT, L., DAUGHRITY, L., BAKER, M. C., RADEMAKERS, R., BOYLAN, K., PATEL, T. C., DICKSON, D. W. & PETRUCELLI, L. 2013. Reduced C9orf72 gene expression in c9FTD/ALS is caused by histone trimethylation, an epigenetic event detectable in blood. *Acta Neuropathol,* 126**,** 895-905.

BENNETT, E. J., MEAD, R. J., AZZOUZ, M., SHAW, P. J. & GRIERSON, A. J. 2014. Early detection of motor dysfunction in the SOD1G93A mouse model of Amyotrophic Lateral Sclerosis (ALS) using home cage running wheels. *PLoS One,* 9**,** e107918.

BROSDA, J., DIETZ, F. & KOCH, M. 2011. Impairment of cognitive performance after reelin knockdown in the medial prefrontal cortex of pubertal or adult rats. *Neurobiol Dis,* 44**,** 239-47.

CHEW, J., GENDRON, T. F., PRUDENCIO, M., SASAGURI, H., ZHANG, Y. J., CASTANEDES-CASEY, M., LEE, C. W., JANSEN-WEST, K., KURTI, A., MURRAY, M. E., BIENIEK, K. F., BAUER, P. O., WHITELAW, E. C., ROUSSEAU, L., STANKOWSKI, J. N., STETLER, C., DAUGHRITY, L. M., PERKERSON, E. A., DESARO, P., JOHNSTON, A., OVERSTREET, K., EDBAUER, D., RADEMAKERS, R., BOYLAN, K. B., DICKSON, D. W., FRYER, J. D. & PETRUCELLI, L. 2015. Neurodegeneration. C9ORF72 repeat expansions in mice cause TDP-43 pathology, neuronal loss, and behavioral deficits. *Science,* 348**,** 1151-4.

COOPER-KNOCK, J., WALSH, M. J., HIGGINBOTTOM, A., ROBIN HIGHLEY, J., DICKMAN, M. J., EDBAUER, D., INCE, P. G., WHARTON, S. B., WILSON, S. A., KIRBY, J., HAUTBERGUE, G. M. & SHAW, P. J. 2014. Sequestration of multiple RNA recognition motif-containing proteins by C9orf72 repeat expansions. *Brain,* 137**,** 2040-51.

DEJESUS-HERNANDEZ, M., MACKENZIE, I. R., BOEVE, B. F., BOXER, A. L., BAKER, M., RUTHERFORD, N. J., NICHOLSON, A. M., FINCH, N. A., FLYNN, H., ADAMSON, J., KOURI, N., WOJTAS, A., SENGDY, P., HSIUNG, G. Y., KARYDAS, A., SEELEY, W. W., JOSEPHS, K. A., COPPOLA, G., GESCHWIND, D. H., WSZOLEK, Z. K., FELDMAN, H., KNOPMAN, D. S., PETERSEN, R. C., MILLER, B. L., DICKSON, D. W., BOYLAN, K. B., GRAFF-RADFORD, N. R. & RADEMAKERS, R. 2011. Expanded

GGGGCC hexanucleotide repeat in noncoding region of C9ORF72 causes chromosome 9p-linked FTD and ALS. *Neuron,* 72**,** 245-56.

DONNELLY, C. J., ZHANG, P. W., PHAM, J. T., HAEUSLER, A. R., MISTRY, N. A., VIDENSKY, S., DALEY, E. L., POTH, E. M., HOOVER, B., FINES, D. M., MARAGAKIS, N., TIENARI, P. J., PETRUCELLI, L., TRAYNOR, B. J., WANG, J., RIGO, F., BENNETT, C. F., BLACKSHAW, S., SATTLER, R. & ROTHSTEIN, J. D. 2013. RNA toxicity from the ALS/FTD C9ORF72 expansion is mitigated by antisense intervention. *Neuron,* 80**,** 415-28.

FREIBAUM, B. D., LU, Y., LOPEZ-GONZALEZ, R., KIM, N. C., ALMEIDA, S., LEE, K. H., BADDERS, N., VALENTINE, M., MILLER, B. L., WONG, P. C., PETRUCELLI, L., KIM, H. J., GAO, F. B. & TAYLOR, J. P. 2015. GGGGCC repeat expansion in C9orf72 compromises nucleocytoplasmic transport. *Nature,* 525**,** 129-33.

FREY, D., SCHNEIDER, C., XU, L., BORG, J., SPOOREN, W. & CARONI, P. 2000. Early and selective loss of neuromuscular synapse subtypes with low sprouting competence in motoneuron diseases. *J Neurosci,* 20**,** 2534-42.

HOWELL, B. W., HAWKES, R., SORIANO, P. & COOPER, J. A. 1997. Neuronal position in the developing brain is regulated by mouse disabled-1. *Nature,* 389**,** 733-7.

IGUCHI, Y., KATSUNO, M., NIWA, J., TAKAGI, S., ISHIGAKI, S., IKENAKA, K., KAWAI, K., WATANABE, H., YAMANAKA, K., TAKAHASHI, R., MISAWA, H., SASAKI, S., TANAKA, F. & SOBUE, G. 2013. Loss of TDP-43 causes age-dependent progressive motor neuron degeneration. *Brain,* 136**,** 1371-82.

JIANG, J., ZHU, Q., GENDRON, T. F., SABERI, S., MCALONIS-DOWNES, M., SEELMAN, A., STAUFFER, J. E., JAFAR-NEJAD, P., DRENNER, K., SCHULTE, D., CHUN, S., SUN, S., LING, S. C., MYERS, B., ENGELHARDT, J., KATZ, M., BAUGHN, M., PLATOSHYN, O., MARSALA, M., WATT, A., HEYSER, C. J., ARD, M. C., DE MUYNCK, L., DAUGHRITY, L. M., SWING, D. A., TESSAROLLO, L., JUNG, C. J., DELPOUX, A., UTZSCHNEIDER, D. T., HEDRICK, S. M., DE JONG, P. J., EDBAUER, D., VAN DAMME, P., PETRUCELLI, L., SHAW, C. E., BENNETT, C. F., DA CRUZ, S., RAVITS, J., RIGO, F., CLEVELAND, D. W. & LAGIER-TOURENNE, C. 2016. Gain of Toxicity from ALS/FTD-Linked Repeat Expansions in C9ORF72 Is Alleviated by Antisense Oligonucleotides Targeting GGGGCC-Containing RNAs. *Neuron,* 90**,** 535-50.

KONG, L., WANG, X., CHOE, D. W., POLLEY, M., BURNETT, B. G., BOSCH-MARCÉ, M., GRIFFIN, J. W., RICH, M. M. & SUMNER, C. J. 2009. Impaired synaptic vesicle release and immaturity of neuromuscular junctions in spinal muscular atrophy mice. *J Neurosci,* 29**,** 842-51.

KOPPERS, M., BLOKHUIS, A. M., WESTENENG, H. J., TERPSTRA, M. L., ZUNDEL, C. A., VIEIRA DE SA, R., SCHELLEVIS, R. D., WAITE, A. J., BLAKE, D. J., VELDINK, J. H., VAN DEN BERG, L. H. & PASTERKAMP, R. J. 2015. C9orf72 ablation in mice does not cause motor neuron degeneration or motor deficits. *Ann Neurol,* 78**,** 426-38.

LEE, K. H., ZHANG, P., KIM, H. J., MITREA, D. M., SARKAR, M., FREIBAUM, B. D., CIKA, J., COUGHLIN, M., MESSING, J., MOLLIEX, A., MAXWELL, B. A., KIM, N. C., TEMIROV, J., MOORE, J., KOLAITIS, R. M., SHAW, T. I., BAI, B., PENG, J., KRIWACKI, R. W. & TAYLOR, J. P. 2016. C9orf72 Dipeptide Repeats Impair the Assembly, Dynamics, and Function of Membrane-Less Organelles. *Cell,* 167**,** 774-788 e17.

LEGER, M., QUIEDEVILLE, A., BOUET, V., HAELEWYN, B., BOULOUARD, M., SCHUMANN-BARD, P. & FRERET, T. 2013. Object recognition test in mice. *Nat Protoc,* 8**,** 2531-7.

LIU, Y., PATTAMATTA, A., ZU, T., REID, T., BARDHI, O., BORCHELT, D. R., YACHNIS, A. T. & RANUM, L. P. 2016. C9orf72 BAC Mouse Model with Motor Deficits and Neurodegenerative Features of ALS/FTD. *Neuron,* 90**,** 521-34.

LOPEZ-GONZALEZ, R., LU, Y., GENDRON, T. F., KARYDAS, A., TRAN, H., YANG, D., PETRUCELLI, L., MILLER, B. L., ALMEIDA, S. & GAO, F. B. 2016. Poly(GR) in C9ORF72-Related ALS/FTD Compromises Mitochondrial Function and Increases Oxidative Stress and DNA Damage in iPSC-Derived Motor Neurons. *Neuron,* 92**,** 383-391.

LOSEN, M., STASSEN, M. H., MARTÍNEZ-MARTÍNEZ, P., MACHIELS, B. M., DUIMEL, H., FREDERIK, P., VELDMAN, H., WOKKE, J. H., SPAANS, F., VINCENT, A. & DE BAETS, M. H. 2005. Increased expression of rapsyn in muscles prevents acetylcholine receptor loss in experimental autoimmune myasthenia gravis. *Brain,* 128**,** 2327-37.

LUKASHCHUK, V., LEWIS, K. E., COLDICOTT, I., GRIERSON, A. J. & AZZOUZ, M. 2016. AAV9-mediated central nervous system-targeted gene delivery via cisterna magna route in mice. *Mol Ther Methods Clin Dev,* 3**,** 15055.

MACKENZIE, I. R., ARZBERGER, T., KREMMER, E., TROOST, D., LORENZL, S., MORI, K., WENG, S. M., HAASS, C., KRETZSCHMAR, H. A., EDBAUER, D. & NEUMANN, M. 2013. Dipeptide repeat protein pathology in C9ORF72 mutation cases: clinico-pathological correlations. *Acta Neuropathol,* 126**,** 859-79.

MAJOUNIE, E., RENTON, A. E., MOK, K., DOPPER, E. G., WAITE, A., ROLLINSON, S., CHIO, A., RESTAGNO, G., NICOLAOU, N., SIMON-SANCHEZ, J., VAN SWIETEN, J. C., ABRAMZON, Y., JOHNSON, J. O., SENDTNER, M., PAMPHLETT, R., ORRELL, R. W., MEAD, S., SIDLE, K. C., HOULDEN, H., ROHRER, J. D., MORRISON, K. E., PALL, H., TALBOT, K., ANSORGE, O., CHROMOSOME, A. L. S. F. T. D. C., FRENCH RESEARCH NETWORK ON, F. F. A., CONSORTIUM, I., HERNANDEZ, D. G., AREPALLI, S., SABATELLI, M., MORA, G., CORBO, M., GIANNINI, F., CALVO, A., ENGLUND, E., BORGHERO, G., FLORIS, G. L., REMES, A. M., LAAKSOVIRTA, H., MCCLUSKEY, L., TROJANOWSKI, J. Q., VAN DEERLIN, V. M., SCHELLENBERG, G. D., NALLS, M. A., DRORY, V. E., LU, C. S., YEH, T. H., ISHIURA, H., TAKAHASHI, Y., TSUJI, S., LE BER, I., BRICE, A., DREPPER, C., WILLIAMS, N., KIRBY, J., SHAW, P., HARDY, J., TIENARI, P. J., HEUTINK, P., MORRIS, H. R., PICKERING-BROWN, S. & TRAYNOR, B. J. 2012. Frequency of the C9orf72 hexanucleotide repeat expansion in

patients with amyotrophic lateral sclerosis and frontotemporal dementia: a cross-sectional study. *Lancet Neurol,* 11**,** 323-30.

MARTINEZ-PENA, Y. V. I., AITTALEB, M., CHEN, P. J. & AKAABOUNE, M. 2015. The knockdown of alphakap alters the postsynaptic apparatus of neuromuscular junctions in living mice. *J Neurosci,* 35**,** 5118-27.

MCCARTY, D. M., MONAHAN, P. E. & SAMULSKI, R. J. 2001. Self-complementary recombinant adeno-associated virus (scAAV) vectors promote efficient transduction independently of DNA synthesis. *Gene Ther,* 8**,** 1248-54.

MEAD, R. J., BENNETT, E. J., KENNERLEY, A. J., SHARP, P., SUNYACH, C., KASHER, P., BERWICK, J., PETTMANN, B., BATTAGLIA, G., AZZOUZ, M., GRIERSON, A. & SHAW, P. J. 2011. Optimised and rapid pre-clinical screening in the SOD1(G93A) transgenic mouse model of amyotrophic lateral sclerosis (ALS). *PLoS One,* 6**,** e23244.

MIZIELINSKA, S., GRONKE, S., NICCOLI, T., RIDLER, C. E., CLAYTON, E. L., DEVOY, A., MOENS, T., NORONA, F. E., WOOLLACOTT, I. O., PIETRZYK, J., CLEVERLEY, K., NICOLL, A. J., PICKERING-BROWN, S., DOLS, J., CABECINHA, M., HENDRICH, O., FRATTA, P., FISHER, E. M., PARTRIDGE, L. & ISAACS, A. M. 2014. C9orf72 repeat expansions cause neurodegeneration in Drosophila through arginine-rich proteins. *Science,* 345**,** 1192-4.

MORI, K., ARZBERGER, T., GRASSER, F. A., GIJSELINCK, I., MAY, S., RENTZSCH, K., WENG, S. M., SCHLUDI, M. H., VAN DER ZEE, J., CRUTS, M., VAN BROECKHOVEN, C., KREMMER, E., KRETZSCHMAR, H. A., HAASS, C. & EDBAUER, D. 2013a. Bidirectional transcripts of the expanded C9orf72 hexanucleotide repeat are translated into aggregating dipeptide repeat proteins. *Acta Neuropathol,* 126**,** 881-93.

MORI, K., WENG, S. M., ARZBERGER, T., MAY, S., RENTZSCH, K., KREMMER, E., SCHMID, B., KRETZSCHMAR, H. A., CRUTS, M., VAN BROECKHOVEN, C., HAASS, C. & EDBAUER, D. 2013b. The C9orf72 GGGGCC repeat is translated into aggregating dipeptide-repeat proteins in FTLD/ALS. *Science,* 339**,** 1335-8.

MURRAY, L. M., TALBOT, K. & GILLINGWATER, T. H. 2010. Review: neuromuscular synaptic vulnerability in motor neurone disease: amyotrophic lateral sclerosis and spinal muscular atrophy. *Neuropathol Appl Neurobiol,* 36**,** 133-56.

O'ROURKE, J. G., BOGDANIK, L., MUHAMMAD, A. K., GENDRON, T. F., KIM, K. J., AUSTIN, A., CADY, J., LIU, E. Y., ZARROW, J., GRANT, S., HO, R., BELL, S., CARMONA, S., SIMPKINSON, M., LALL, D., WU, K., DAUGHRITY, L., DICKSON, D. W., HARMS, M. B., PETRUCELLI, L., LEE, E. B., LUTZ, C. M. & BALOH, R. H. 2015. C9orf72 BAC Transgenic Mice Display Typical Pathologic Features of ALS/FTD. *Neuron,* 88**,** 892-901.

O'ROURKE, J. G., BOGDANIK, L., YANEZ, A., LALL, D., WOLF, A. J., MUHAMMAD, A. K., HO, R., CARMONA, S., VIT, J. P., ZARROW, J., KIM, K. J., BELL, S., HARMS, M. B., MILLER, T. M., DANGLER, C. A., UNDERHILL, D. M., GOODRIDGE, H. S., LUTZ, C. M. & BALOH, R. H. 2016. C9orf72 is required for proper macrophage and microglial function in mice. *Science,* 351**,** 1324-9.

PETERS, O. M., CABRERA, G. T., TRAN, H., GENDRON, T. F., MCKEON, J. E., METTERVILLE, J., WEISS, A., WIGHTMAN, N., SALAMEH, J., KIM, J., SUN, H., BOYLAN, K. B., DICKSON, D., KENNEDY, Z., LIN, Z., ZHANG, Y. J., DAUGHRITY, L., JUNG, C., GAO, F. B., SAPP, P. C., HORVITZ, H. R., BOSCO, D. A., BROWN, S. P., DE JONG, P., PETRUCELLI, L., MUELLER, C. & BROWN, R. H., JR. 2015. Human C9ORF72 Hexanucleotide Expansion Reproduces RNA Foci and Dipeptide Repeat Proteins but Not Neurodegeneration in BAC Transgenic Mice. *Neuron,* 88**,** 902-9.

PLETNIKOVA, O., SLOANE, K. L., RENTON, A. E., TRAYNOR, B. J., CRAIN, B. J., REID, T., ZU, T., RANUM, L. P., TRONCOSO, J. C., RABINS, P. V. & ONYIKE, C. U. 2014. Hippocampal sclerosis dementia with the C9ORF72 hexanucleotide repeat expansion. *Neurobiol Aging,* 35**,** 2419.e17-21.

POWIS, R. A., KARYKA, E., BOYD, P., COME, J., JONES, R. A., ZHENG, Y., SZUNYOGOVA, E., GROEN, E. J., HUNTER, G., THOMSON, D., WISHART, T. M., BECKER, C. G., PARSON, S. H., MARTINAT, C., AZZOUZ, M. & GILLINGWATER, T. H. 2016. Systemic restoration of UBA1 ameliorates disease in spinal muscular atrophy. *JCI Insight,* 1**,** e87908.

PUJADAS, L., ROSSI, D., ANDRÉS, R., TEIXEIRA, C. M., SERRA-VIDAL, B., PARCERISAS, A., MALDONADO, R., GIRALT, E., CARULLA, N. & SORIANO, E. 2014. Reelin delays amyloid-beta fibril formation and rescues cognitive deficits in a model of Alzheimer's disease. *Nat Commun,* 5**,** 3443.

RENTON, A. E., CHIO, A. & TRAYNOR, B. J. 2014. State of play in amyotrophic lateral sclerosis genetics. *Nat Neurosci,* 17**,** 17-23.

RENTON, A. E., MAJOUNIE, E., WAITE, A., SIMON-SANCHEZ, J., ROLLINSON, S., GIBBS, J. R., SCHYMICK, J. C., LAAKSOVIRTA, H., VAN SWIETEN, J. C., MYLLYKANGAS, L., KALIMO, H., PAETAU, A., ABRAMZON, Y., REMES, A. M., KAGANOVICH, A., SCHOLZ, S. W., DUCKWORTH, J., DING, J., HARMER, D. W., HERNANDEZ, D. G., JOHNSON, J. O., MOK, K., RYTEN, M., TRABZUNI, D., GUERREIRO, R. J., ORRELL, R. W., NEAL, J., MURRAY, A., PEARSON, J., JANSEN, I. E., SONDERVAN, D., SEELAAR, H., BLAKE, D., YOUNG, K., HALLIWELL, N., CALLISTER, J. B., TOULSON, G., RICHARDSON, A., GERHARD, A., SNOWDEN, J., MANN, D., NEARY, D., NALLS, M. A., PEURALINNA, T., JANSSON, L., ISOVIITA, V. M., KAIVORINNE, A. L., HOLTTA-VUORI, M., IKONEN, E., SULKAVA, R., BENATAR, M., WUU, J., CHIO, A., RESTAGNO, G., BORGHERO, G., SABATELLI, M., CONSORTIUM, I., HECKERMAN, D., ROGAEVA, E., ZINMAN, L., ROTHSTEIN, J. D., SENDTNER, M., DREPPER, C., EICHLER, E. E., ALKAN, C., ABDULLAEV, Z., PACK, S. D., DUTRA, A., PAK, E., HARDY, J., SINGLETON, A., WILLIAMS, N. M., HEUTINK, P., PICKERING-BROWN, S., MORRIS, H. R., TIENARI, P. J. & TRAYNOR,

B. J. 2011. A hexanucleotide repeat expansion in C9ORF72 is the cause of chromosome 9p21-linked ALS-FTD. *Neuron,* 72**,** 257-68.

SCHLUDI, M. H., MAY, S., GRASSER, F. A., RENTZSCH, K., KREMMER, E., KUPPER, C., KLOPSTOCK, T., GERMAN CONSORTIUM FOR FRONTOTEMPORAL LOBAR, D., BAVARIAN BRAIN BANKING, A., ARZBERGER, T. & EDBAUER, D. 2015. Distribution of dipeptide repeat proteins in cellular models and C9orf72 mutation cases suggests link to transcriptional silencing. *Acta Neuropathol,* 130**,** 537-55.

TRAN, H., ALMEIDA, S., MOORE, J., GENDRON, T. F., CHALASANI, U., LU, Y., DU, X., NICKERSON, J. A., PETRUCELLI, L., WENG, Z. & GAO, F. B. 2015. Differential Toxicity of Nuclear RNA Foci versus Dipeptide Repeat Proteins in a Drosophila Model of C9ORF72 FTD/ALS. *Neuron,* 87**,** 1207-14.

TROMMSDORFF, M., GOTTHARDT, M., HIESBERGER, T., SHELTON, J., STOCKINGER, W., NIMPF, J., HAMMER, R. E., RICHARDSON, J. A. & HERZ, J. 1999. Reeler/Disabled-like disruption of neuronal migration in knockout mice lacking the VLDL receptor and ApoE receptor 2. *Cell,* 97**,** 689-701.

TURNEY, S. G., CULICAN, S. M. & LICHTMAN, J. W. 1996. A quantitative fluorescence-imaging technique for studying acetylcholine receptor turnover at neuromuscular junctions in living animals. *J Neurosci Methods,* 64**,** 199-208.

WISHART, T. M., MUTSAERS, C. A., RIESSLAND, M., REIMER, M. M., HUNTER, G., HANNAM, M. L., EATON, S. L., FULLER, H. R., ROCHE, S. L., SOMERS, E., MORSE, R., YOUNG, P. J., LAMONT, D. J., HAMMERSCHMIDT, M., JOSHI, A., HOHENSTEIN, P., MORRIS, G. E., PARSON, S. H., SKEHEL, P. A., BECKER, T., ROBINSON, I. M., BECKER, C. G., WIRTH, B. & GILLINGWATER, T. H. 2014. Dysregulation of ubiquitin homeostasis and beta-catenin signaling promote spinal muscular atrophy. *J Clin Invest,* 124**,** 1821-34.

ZHANG, K., DONNELLY, C. J., HAEUSLER, A. R., GRIMA, J. C., MACHAMER, J. B., STEINWALD, P., DALEY, E. L., MILLER, S. J., CUNNINGHAM, K. M., VIDENSKY, S., GUPTA, S., THOMAS, M. A., HONG, I., CHIU, S. L., HUGANIR, R. L., OSTROW, L. W., MATUNIS, M. J., WANG, J., SATTLER, R., LLOYD, T. E. & ROTHSTEIN, J. D. 2015. The C9orf72 repeat expansion disrupts nucleocytoplasmic transport. *Nature,* 525**,** 56-61.

ZU, T., GIBBENS, B., DOTY, N. S., GOMES-PEREIRA, M., HUGUET, A., STONE, M. D., MARGOLIS, J., PETERSON, M., MARKOWSKI, T. W., INGRAM, M. A., NAN, Z., FORSTER, C., LOW, W. C., SCHOSER, B., SOMIA, N. V., CLARK, H. B., SCHMECHEL, S., BITTERMAN, P. B., GOURDON, G., SWANSON, M. S., MOSELEY, M. & RANUM, L. P. 2011. Non-ATG-initiated translation directed by microsatellite expansions. *Proc Natl Acad Sci U S A,* 108**,** 260-5.

Figure 1

A

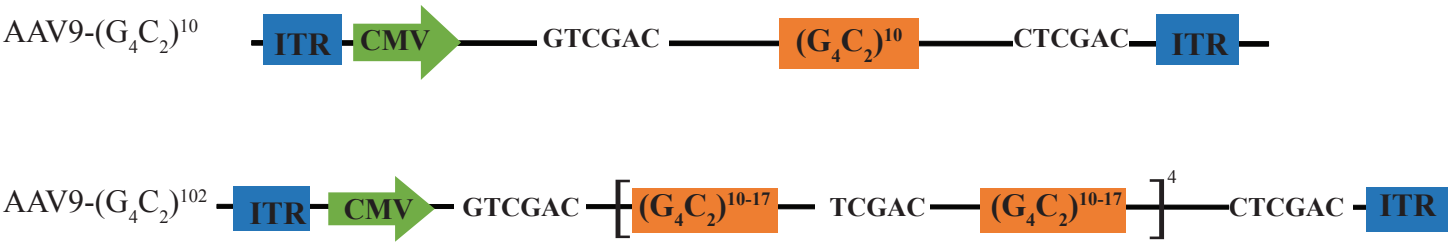
AAV9-(G4C2)10
ITR
CMV
GTCGAC
(G4C2)10
CTCGAC
ITR
AAV9-(G4C2)102
ITR
CMV
GTCGAC
(G4C2)10-17
TCGAC
(G4C2)10-17
4
CTCGAC
ITR

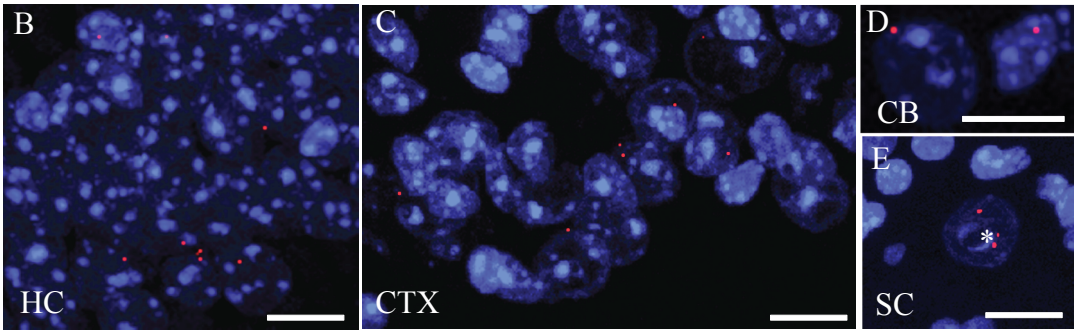
B
HC
C
CTX
D
CB
E
SC

F

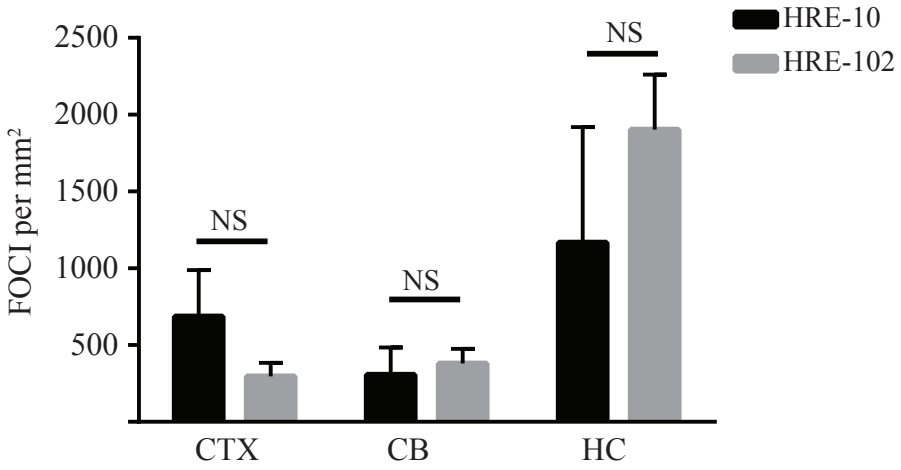
HRE-10
HRE-102
FOCI per mm2
2500
2000
1500
1000
500
NS
NS
NS
CTX
CB
HC

Figure 2

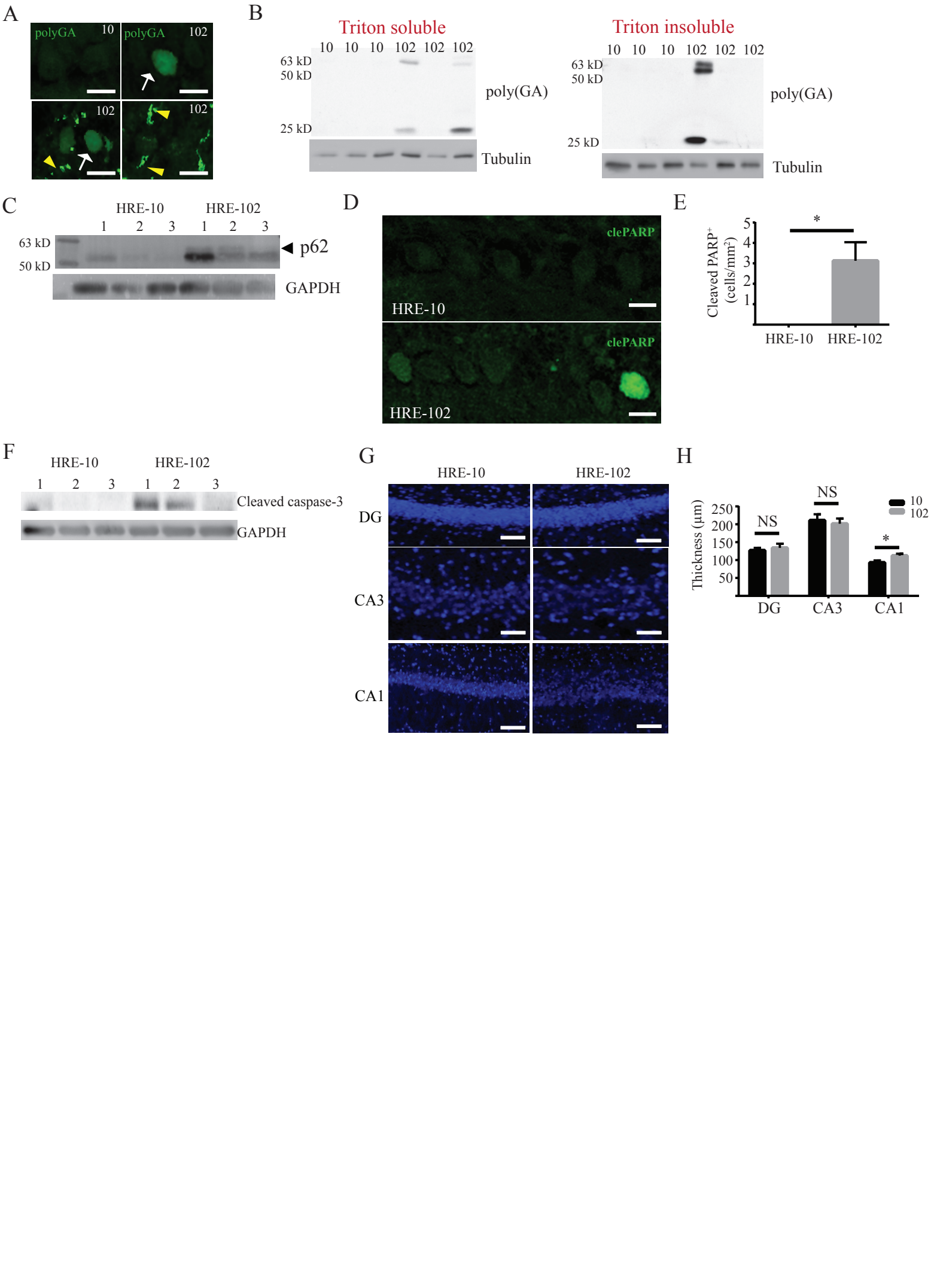
A
polyGA 10
polyGA 102
102
102
B
Triton soluble
10 10 10 102 102 102
63 kD
50 kD
25 kD
poly(GA)
Tubulin
Triton insoluble
10 10 10 102 102 102
63 kD
50 kD
25 kD
poly(GA)
Tubulin
C
HRE-10
HRE-102
1 2 3 1 2 3
63 kD
50 kD
p62
GAPDH
D
clePARP
HRE-10
clePARP
HRE-102
E
Cleaved PARP+ (cells/mm2)
5
4
3
2
1
*
HRE-10
HRE-102
F
HRE-10
HRE-102
1 2 3 1 2 3
Cleaved caspase-3
GAPDH
G
HRE-10
HRE-102
DG
CA3
CA1
H
Thickness (μm)
250
200
150
100
50
NS
NS
*
10
102
DG
CA3
CA1

Figure 3

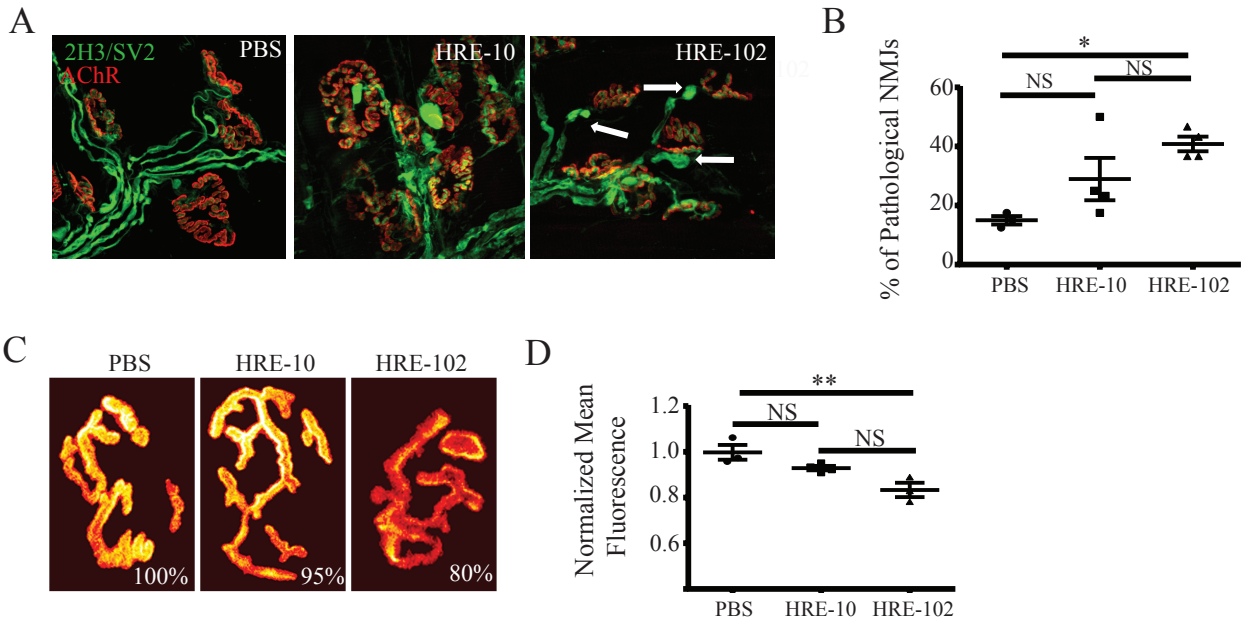
A
2H3/SV2
AChR
PBS
HRE-10
HRE-102
B
% of Pathological NMJs
60
40
20
0
*
NS
NS
PBS
HRE-10
HRE-102
C
PBS
HRE-10
HRE-102
100%
95%
80%
D
Normalized Mean Fluorescence
1.2
1.0
0.8
0.6
**
NS
NS
PBS
HRE-10
HRE-102

Figure 4

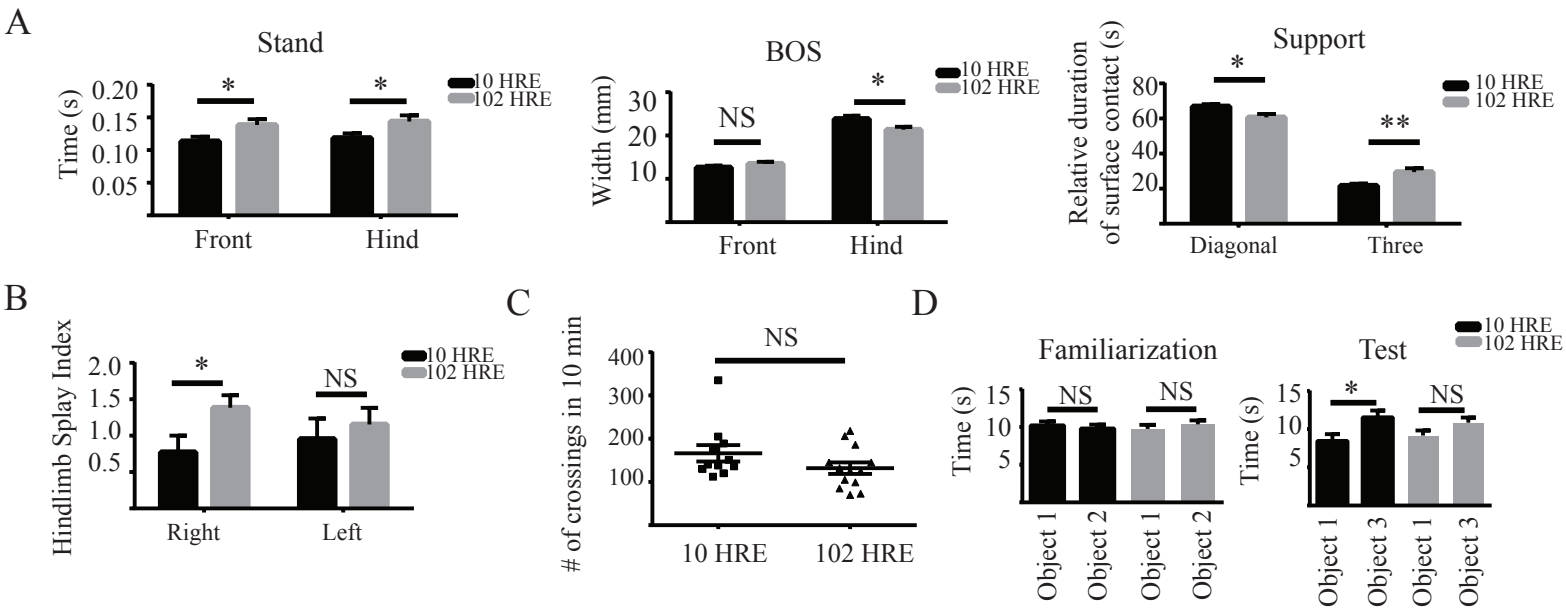
A
Stand
Time (s)
0.20
0.15
0.10
0.05
*
*
10 HRE
102 HRE
Front
Hind
BOS
Width (mm)
30
20
10
NS
*
10 HRE
102 HRE
Front
Hind
Support
Relative duration of surface contact (s)
80
60
40
20
*
**
10 HRE
102 HRE
Diagonal
Three
B
Hindlimb Splay Index
2.0
1.5
1.0
0.5
*
NS
10 HRE
102 HRE
Right
Left
C
# of crossings in 10 min
400
300
200
100
NS
10 HRE
102 HRE
D
Familiarization
Test
10 HRE
102 HRE
Time (s)
15
10
5
NS
NS
*
NS
Object 1
Object 2
Object 1
Object 2
Object 1
Object 3
Object 1
Object 3